Exact general relativistic rotating thick disks

D. Vogt* and P. S. Letelier†

Departamento de Matemática Aplicada-IMECC, Universidade Estadual de Campinas, 13083-970 Campinas, S.P., Brazil

(Received 23 May 2007; revised manuscript received 16 August 2007; published 12 October 2007)

Two families of exact general relativistic rotating thick disks based on the Kerr metric are obtained by applying two kinds of transformation on the Kerr solution. The first is the one proposed by Miyamoto and Nagai in the context of Newtonian galactic models, and the second one is based on the ''displace, cut, fill and reflect'' method. Both kinds of disks have well-behaved energy-density distributions. A stability analysis of circular orbits on the $z = 0$ plane shows that for large values of the Kerr parameter some retrograde orbits tend to be unstable.

DOI: 10.1103/PhysRevD.76.084010 PACS numbers: 04.20.Jb, 04.40.−b

I. INTRODUCTION

Exact solutions of Einstein's field equations with axial symmetry play an important role in the astrophysical applications of general relativity, since the natural shape of an isolated self-gravitating fluid is axially symmetric. In particular, disklike configurations of matter are of great interest, since they can be used as models of galaxies and accretion disks. In past decades, several disklike solutions were found. Solutions for static thin disks without radial pressure were first studied by Bonnor and Sackfield [1], and Morgan and Morgan [2]. Disks with radial pressure were considered by Morgan and Morgan [3], and González and Letelier [4]. Several other classes of exact solutions of the Einstein field equations corresponding to static thin disks with or without radial pressure have been obtained by different authors [5–14]. Thin rotating disks that can be considered as a source of the Kerr metric were presented in [15], while rotating disks with heat flow were studied in [16]. Also thin disks with magnetic fields [17] and magnetic and electric fields [18] were considered. The nonlinear superposition of a disk and a black hole was first obtained by Lemos and Letelier [8]. Perfect fluid disks with halos [19] and charged perfect fluid disks [20] were also studied. For a survey on self-gravitating relativistic thin disks, see for instance [21].

In the works cited above, an inverse style method was used to solve the Einstein equations, i.e., the energy-momentum tensor is computed from the metric representing the disk. Another approach to generate disks is by solving the Einstein equations given a source (energy-momentum tensor). This has been used by different authors to generate several exact solutions of thin disks [22–29].

Even though in a first approximation thin disks can be used as useful models of galaxies, in a more realistic model the thickness of the disk should be considered. The addition of a new dimension may change the dynamical properties of the disk source, e.g., its stability. Thick static relativistic disks in various coordinate systems were presented in [30,31]. Also a relativistic generalization of the Miyamoto-Nagai potential-density pairs [32,33] was studied in [34].

An important question concerning disk models is its stability. In general relativistic disks there are usually two approaches to address this question. One is to study the stability of test particles along geodesics by using a generalization of the Rayleigh criteria of stability [35] of a fluid at rest in a gravitational field, as was done, for example, by Letelier [36]. The other way to study stability of disks is by analyzing the conservation equations obtained from perturbations of the components of the disk's energy-momentum tensor. This kind of study was made by Ujevic and Letelier [37] on thin disks and also on a model of a thick disk in isotropic coordinates [38].

In this work we add a new degree of reality to the simple models of galaxies and consider relativistic rotating thick disks. In particular, the Kerr metric is used to construct two families of disks. One is obtained by applying a transformation proposed by Miyamoto and Nagai [32,33]. The other is based on the ''displace, cut, fill and reflect'' method that was used in [30,31] to generate static thick disks. The work is divided as follows. In Sec. II we present the main physical quantities associated to the disk. In Sec. III the properties of the disks obtained from the above-mentioned transformations are discussed. The rotation curves and stability of test particles along circular geodesics on the galactic plane are also discussed. Finally, in Sec. IV we summarize the main results and make some comments.

II. ROTATING RELATIVISTIC THICK DISKS

In this section we present a summary of the main quantities associated to the disk; we follow closely Ref. [16]. When matter is absent, the metric for a stationary axially symmetric spacetime can be cast as

$$ds^2 = -e^{2\Phi}(dt + \mathcal{A}d\varphi)^2 + e^{-2\Phi}[r^2 d\varphi^2 + e^{2\Lambda}(dr^2 + dz^2)], \quad (1)$$

where Φ, Λ, and $\mathcal{A}$ are functions of r and z only. The

*dvogt@ime.unicamp.br
†letelier@ime.unicamp.br

Einstein vacuum equations for this metric yield

$$\Phi_{,rr} + \frac{\Phi_{,r}}{r} + \Phi_{,zz} + \frac{e^{4\Phi}}{2r^2}(\mathcal{A}_{,r}^2 + \mathcal{A}_{,z}^2) = 0, \tag{2}$$

$$\mathcal{A}_{,rr} - \frac{\mathcal{A}_{,r}}{r} + \mathcal{A}_{,zz} + 4(\Phi_{,r}\mathcal{A}_{,r} + \Phi_{,z}\mathcal{A}_{,z}), \tag{3}$$

$$\Lambda_{,r} = r(\Phi_{,r}^2 - \Phi_{,z}^2) - \frac{e^{4\Phi}}{4r}(\mathcal{A}_{,r}^2 - \mathcal{A}_{,z}^2), \tag{4}$$

$$\Lambda_{,z} = 2r\Phi_{,r}\Phi_{,z} - \frac{e^{4\Phi}}{2r}\mathcal{A}_{,r}\mathcal{A}_{,z}. \tag{5}$$

From a solution of Eqs. (2)–(5), we can construct a thick stationary disk using the transformation $z \to h(z) + a$, where a is a constant and $h(z)$ an even function of z. Two particular functional forms for $h(z)$ will be discussed later. The resulting energy-momentum tensor of the disk can be computed using the Einstein equations,

$$T_{ab} = R_{ab} - \tfrac{1}{2}Rg_{ab}, \tag{6}$$

where we use units such that $c = 8\pi G = 1$. By using the vacuum equations (2)–(5), the nonzero components of T_b^a are

$$\begin{aligned} T_t^t = {} & \frac{e^{6\Phi-2\Lambda}}{r^2}\Big[-\frac{\mathcal{A}}{2}\mathcal{A}_{,h}h'' + (1-h'^2) \\ & \times\Big(\frac{\mathcal{A}}{2}\mathcal{A}_{,hh} + 2\mathcal{A}\mathcal{A}_{,h}\Phi_{,h} + \frac{3}{4}\mathcal{A}_{,h}^2\Big)\Big] \\ & + e^{2\Phi-2\Lambda}[h''(\Lambda_{,h} - 2\Phi_{,h}) \\ & - (1-h'^2)(\Lambda_{,hh} - 2\Phi_{,hh} + \Phi_{,h}^2)], \end{aligned} \tag{7}$$

$$\begin{aligned} T_\varphi^t = {} & \frac{e^{6\Phi-2\Lambda}\mathcal{A}}{2r^2}[-\mathcal{A}\mathcal{A}_{,h}h'' + (1-h'^2) \\ & \times(2\mathcal{A}_{,h}^2 + \mathcal{A}\mathcal{A}_{,hh} + 4\mathcal{A}\mathcal{A}_{,h}\Phi_{,h})] \\ & + \frac{e^{2\Phi-2\Lambda}}{2}[-h''(\mathcal{A}_{,h} + 4\mathcal{A}\Phi_{,h}) \\ & + (1-h'^2)(\mathcal{A}_{,hh} + 4\mathcal{A}\Phi_{,hh} + 4\mathcal{A}_{,h}\Phi_{,h})], \end{aligned} \tag{8}$$

$$T_t^\varphi = \frac{e^{6\Phi-2\Lambda}}{2r^2}[\mathcal{A}_{,h}h'' - (1-h'^2)(\mathcal{A}_{,hh} + 4\mathcal{A}_{,h}\Phi_{,h})], \tag{9}$$

$$\begin{aligned} T_\varphi^\varphi = {} & \frac{e^{6\Phi-2\Lambda}}{2r^2}\Big[\mathcal{A}\mathcal{A}_{,h}h'' - (1-h'^2) \\ & \times\Big(\mathcal{A}\mathcal{A}_{,h} + 4\mathcal{A}\mathcal{A}_{,h}\Phi_{,h} + \frac{\mathcal{A}_{,h}^2}{2}\Big)\Big] \\ & + e^{2\Phi-2\Lambda}[\Lambda_{,h}h'' - (1-h'^2)(\Lambda_{,hh} + \Phi_{,h}^2)], \end{aligned} \tag{10}$$

$$T_r^r = -T_z^z = (1-h'^2)\Big[\frac{e^{6\Phi-2\Lambda}}{4r^2}\mathcal{A}_{,h}^2 - e^{2\Phi-2\Lambda}\Phi_{,h}^2\Big], \tag{11}$$

where primes indicate differentiation with respect to z. The physical quantities associated to the matter distribution are obtained by solving the eigenvalue problem for the energy-momentum tensor $T_b^a\xi^b = \lambda\xi^a$:

$$\lambda_\pm = \tfrac{1}{2}(T \pm \sqrt{D}), \tag{12}$$

$$T = T_t^t + T_\varphi^\varphi, \qquad D = (T_\varphi^\varphi - T_t^t)^2 + 4T_\varphi^t T_t^\varphi, \tag{13}$$

$$\lambda_r = T_r^r, \qquad \lambda_z = T_z^z. \tag{14}$$

The canonical form of the energy-momentum tensor is

$$\begin{aligned} T_{ab} = {} & \epsilon V_a V_b + P_\varphi W_a W_b + \kappa(V_a W_b + W_a V_b) \\ & + P_r X_a X_b + P_z Y_a Y_b, \end{aligned} \tag{15}$$

with an orthonormal basis $\{V^a, W^a, X^a, Y^a\}$, where $V^a = N_0(1, \Omega, 0, 0)$, $W^a = N_1(\Delta, 1, 0, 0)$, $Y^a = e^{\Phi-\Lambda}(0, 0, 1, 0)$, and $Z^a = e^{\Phi-\Lambda}(0, 0, 0, 1)$. Here N_0 and N_1 are normalization factors, and

$$\Omega = \begin{cases} (\lambda_- - T_t^t)/T_\varphi^t, & D \geq 0, \\ (T_\varphi^\varphi)/(2T_\varphi^t), & D < 0, \end{cases} \tag{16}$$

$$\Delta = \begin{cases} (\lambda_+ - T_\varphi^\varphi)/T_t^\varphi, & D \geq 0, \\ 0, & D < 0. \end{cases} \tag{17}$$

The energy density, the azimuthal stress, the heat flow function, and the vertical and radial stresses are, respectively,

$$\epsilon = \begin{cases} -\lambda_-, & D \geq 0, \\ -T/2, & D < 0, \end{cases} \tag{18}$$

$$P_\varphi = \begin{cases} \lambda_+, & D \geq 0, \\ T/2, & D < 0, \end{cases} \tag{19}$$

$$\kappa = \begin{cases} 0, & D \geq 0, \\ -\sqrt{D}/2, & D < 0, \end{cases} \tag{20}$$

$$P_z = T_z^z, \qquad P_r = T_r^r = -P_z. \tag{21}$$

When there is no heat flow, the "effective Newtonian" density is given by $\rho = \epsilon + P_\varphi + P_r + P_z = \sqrt{D}$. To satisfy the strong energy condition we must have $\rho \geq 0$, the weak energy condition requires $\epsilon \geq 0$, and the dominant energy condition requires $|P_\varphi/\epsilon| \leq 1$, $|P_r/\epsilon| \leq 1$, and $|P_z/\epsilon| \leq 1$ [39].

A rotation profile (tangential velocity) of test particles can be calculated by assuming circular motion along geodesics on the galactic plane (located on $z = 0$). This assumption is valid for the case of a particle moving in a very diluted gas like the gas made of stars that models a galactic

disk. Let $u^a = u^0(1, \omega, 0, 0)$ be the velocity vector of a test particle. The expression for the angular velocity ω follows from the geodesic equation for the r coordinate,

$$g_{\varphi\varphi,r}\omega^2 + 2g_{t\varphi,r}\omega + g_{tt,r} = 0, \tag{22}$$

whose solutions are

$$\omega_\pm = \frac{-g_{t\varphi,r} \pm \sqrt{g_{t\varphi,r}^2 - g_{tt,r}g_{\varphi\varphi,r}}}{g_{\varphi\varphi,r}}. \tag{23}$$

Therefore, in general, the prograde and retrograde angular velocities are different. The tangential velocity can be calculated by projecting the velocity vector u^a onto the tetrad $e^b_{\hat{a}} = \{V^b, W^b, X^b, Y^b\}$:

$$u^{\hat{a}} = e^{\hat{a}}{}_b u^b = \eta^{\hat{a}\hat{c}} e_{\hat{c}b} u^b. \tag{24}$$

Thus

$$U_\pm = \frac{u^{\hat{\varphi}}}{u^{\hat{t}}} = -\frac{W_t + W_\varphi \omega_\pm}{V_t + V_\varphi \omega_\pm}, \tag{25}$$

where all functions are evaluated on $z = 0$.

The specific angular momentum per unit mass of a test particle is given by $\mathsf{h} = g_{\varphi a}u^a$. The angular momentum can be used to determine the stability of circular orbits on the galactic plane by using an extension of the Rayleigh criteria of stability [35] of a fluid at rest in a gravitational field,

$$\left.\frac{d\mathsf{h}^2}{dr}\right|_{z=0} > 0. \tag{26}$$

III. THICK KERR DISKS

In this section we study two families of thick rotating disks constructed from the Kerr solution, which can be written as

$$\Phi = \frac{1}{2}\ln\left[\frac{(R_1 + R_2)^2 - 4m^2 + \alpha^2(R_1 - R_2)^2/\sigma^2}{(R_1 + R_2 + 2m)^2 + \alpha^2(R_1 - R_2)^2/\sigma^2}\right], \tag{27}$$

$$\Lambda = \frac{1}{2}\ln\left[\frac{(R_1 + R_2)^2 - 4m^2 + \alpha^2(R_1 - R_2)^2/\sigma^2}{4R_1R_2}\right], \tag{28}$$

$$\mathcal{A} = \frac{\alpha m}{\sigma^2}\frac{(R_1 + R_2 + 2m)[4\sigma^2 - (R_1 - R_2)^2]}{(R_1 + R_2)^2 - 4m^2 + \alpha^2(R_1 - R_2)^2/\sigma^2}, \tag{29}$$

where m and α are the mass and Kerr parameter, respec-

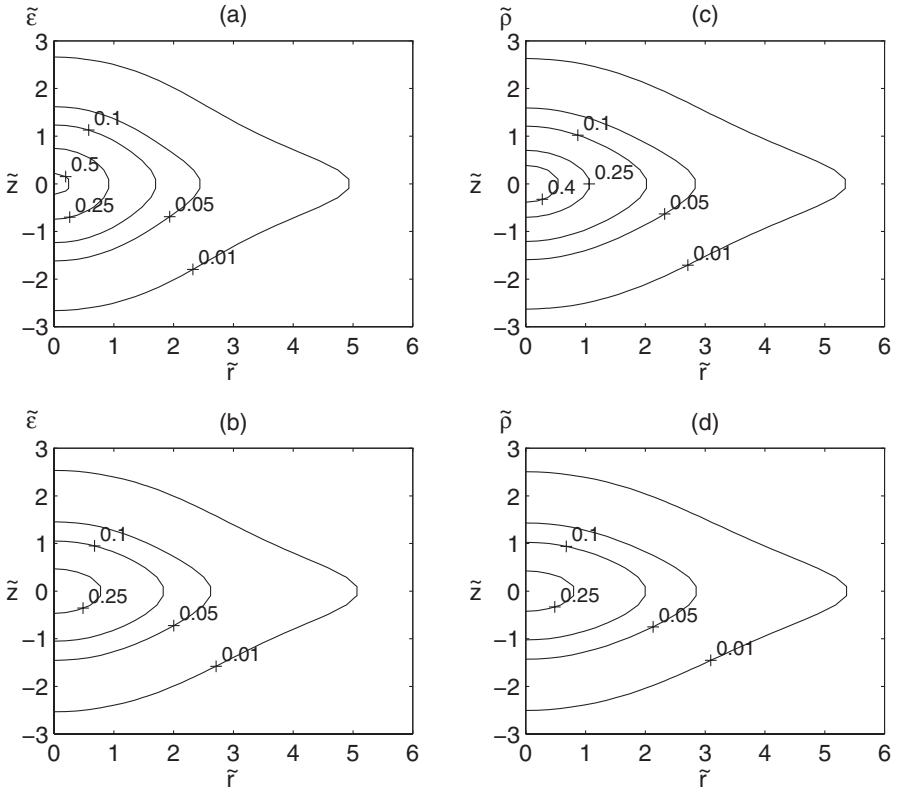

FIG. 1. For the Miyamoto-Nagai–like Kerr disk, we show level curves of the energy density $\tilde{\epsilon}$ as functions of $\tilde{r}$ and $\tilde{z}$ with parameters $\tilde{a} = 1$, $\tilde{b} = 1$, $\tilde{\alpha} = 0.1$ in (a) and $\tilde{\alpha} = 0.9$ in (b). The effective Newtonian density $\tilde{\rho}$ with the same parameters is shown in (c) and (d).

tively, $R_1 = \sqrt{r^2 + (z+\sigma)^2}$, $R_2 = \sqrt{r^2 + (z-\sigma)^2}$, and $\sigma = \sqrt{m^2 - \alpha^2}$.

A. A Miyamoto-Nagai–like Kerr disk

We use a transformation first proposed by Miyamoto and Nagai [32,33] to generate potential-density pairs useful for modeling both the central bulge and the disk part of galaxies. It consists in replacing z by $a + \sqrt{z^2 + b^2}$, where a and b are non-negative parameters. When this transformation is applied on the solution (27)–(29), Eqs. (7)–(21) generate exact but huge expressions that will not be presented. The analysis is better done graphically. Figures 1(a) and 1(b) show some level curves of the energy density $\tilde{\epsilon} = m^2\epsilon$ with parameters $\tilde{a} = a/m = 1$, $\tilde{b} = b/m = 1$, $\tilde{\alpha} = \alpha/m = 0.1$ (slow rotation) in (a) and $\tilde{\alpha} = 0.9$ (high rotation) in (b). In Figs. 1(c) and 1(d), we display level curves of the effective Newtonian density $\tilde{\rho} = m^2\rho$ with the same parameters. The discriminant D is everywhere non-negative, thus there is no heat flow. We also found $D \geq 0$ for several other values of the parameters. The density distributions are non-negative, free from singularities, and decay along the radial direction as well as the vertical direction. As the Kerr parameter increases, the density distributions become slightly flattened and the maximum values at the origin decrease. The level curves for azimuthal stress and vertical stress are displayed in Figs. 2(a)–2(d), respectively, with the same parameters as in Fig. 1. Near the disk's center we have azimuthal tension and for larger values of r and z azimuthal pressure. Thus there is a solid core surrounded by a fluid. The maximum of pressure is shifted to the right as the Kerr parameter is increased. From Figs. 2(c) and 2(d) we have vertical pressure which has the same modulus as radial tension. Therefore, the disk is composed of an anisotropic fluid with regions of shear tensions. For $\tilde{\alpha} = 0.1$ we have $|\tilde{P}_\varphi/\tilde{\epsilon}| < 0.4$, $|\tilde{P}_z/\tilde{\epsilon}| < 0.1$; for $\tilde{\alpha} = 0.9$ we have $|\tilde{P}_\varphi/\tilde{\epsilon}| < 0.3$ and $|\tilde{P}_z/\tilde{\epsilon}| < 0.06$; thus the dominant energy condition is also satisfied.

In Fig. 3(a) we depict some curves of the prograde tangential velocity U_+ and retrograde tangential velocity U_- for the Miyamoto-Nagai–like Kerr disk with $\tilde{a} = 1$, $\tilde{b} = 1$, $\tilde{\alpha} = 0.1$ (solid lines), $\tilde{\alpha} = 0.5$ (dashed lines), and $\tilde{\alpha} = 0.9$ (dotted lines). Figure 3(b) shows the curves of the square of angular momenta h_-^2 (upper curves) and h_+^2 (lower curves) with the same parameters. The same quantities are repeated in Figs. 3(c) and 3(d) but now with parameter $\tilde{b} = 0.5$. By high rotation the prograde and retrograde velocity curves become more asymmetric. From the Rayleigh criteria of stability, we note that the circular orbits are almost stable for the parameters shown.

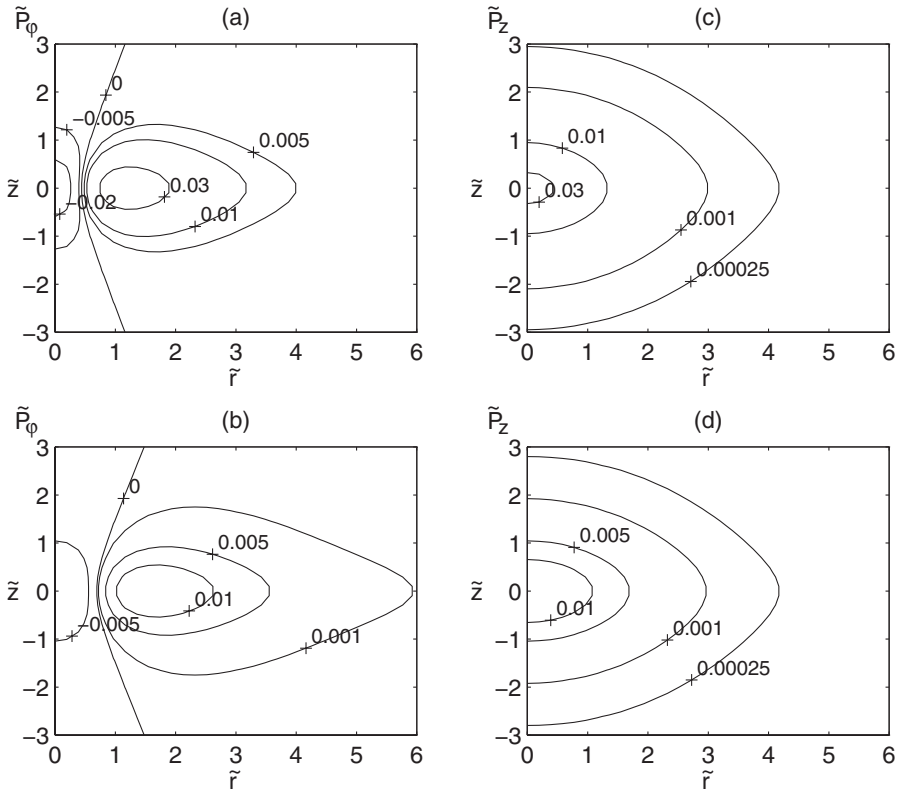

FIG. 2. For the Miyamoto-Nagai–like Kerr disk, we show level curves of the azimuthal stress $\tilde{P}_\varphi$ as functions of $\tilde{r}$ and $\tilde{z}$ with parameters $\tilde{a} = 1$, $\tilde{b} = 1$, $\tilde{\alpha} = 0.1$ in (a) and $\tilde{\alpha} = 0.9$ in (b). The vertical pressure $\tilde{P}_z$ with the same parameters is shown in (c) and (d).

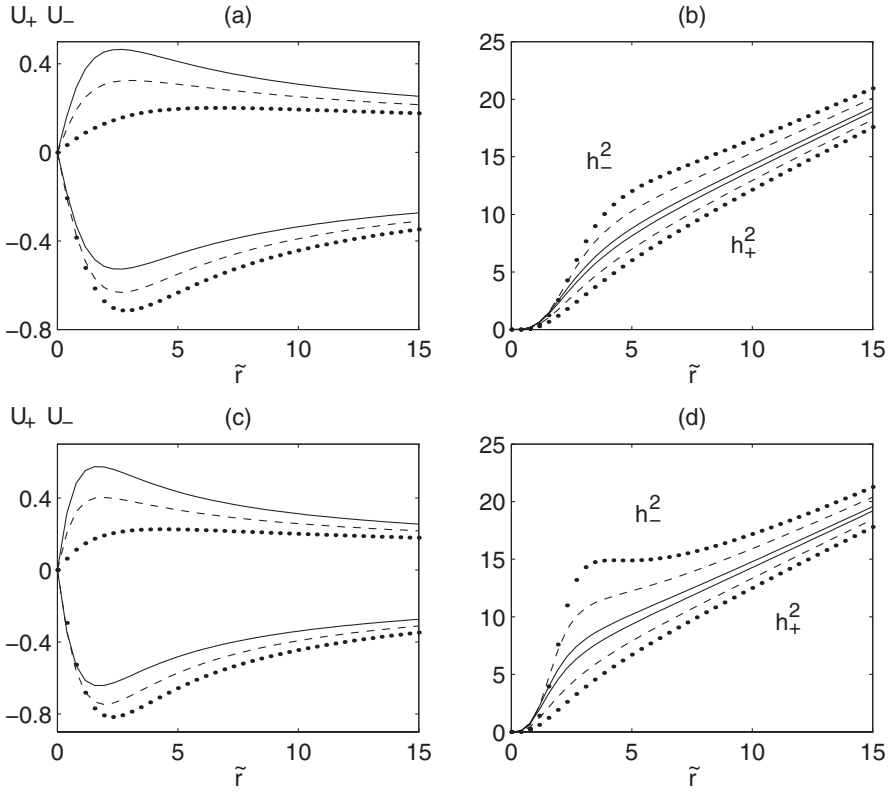

FIG. 3. For the Miyamoto-Nagai–like Kerr disk, we show curves of the prograde U_+ and retrograde U_- tangential velocities and the square of angular momenta h_-^2 and h_+^2. Parameters: $\tilde{a} = 1$, $\tilde{\alpha} = 0.1$ (solid lines), $\tilde{\alpha} = 0.5$ (dashed lines), $\tilde{\alpha} = 0.9$ (dotted lines), $\tilde{b} = 1$ in (a) and (b) and $\tilde{b} = 0.5$ in (c) and (d).

However, in Fig. 3(d) a small region of instability appears for retrogade motion near $\tilde{r} = 5$.

B. A second family of thick Kerr disks

Another family of rotating thick disks can be constructed with the "displace, cut, fill and reflect" method used in [30,31] to generate static thick disks. This can be divided in the following steps: (i) cut the spacetime above its singularities, then disregard the part of the spacetime containing the singularities; (ii) put a thick shell below the surface; and (iii) use the bottom surface of the shell to make an inversion. The mathematical equivalent is a transformation $z \longrightarrow h(z) + a$, where we use an even polynomial class of functions given by

$$h(z) = \begin{cases} -z + C, & z \le -b, \\ Az^2 + Bz^{2n+2}, & -b \le z \le b, \\ z + C, & z \ge b, \end{cases} \qquad (30)$$

with

$$A = \frac{2n + 1 - bc}{4nb}, \qquad B = \frac{bc - 1}{4n(n+1)b^{2n+1}},$$
$$C = -\frac{b(2n + 1 + bc)}{4(n+1)}.$$

Here $n = 1, 2, \ldots, b$ is the disk half-thickness and c is the jump of the second derivative on $z = \pm b$. The specific form of this class of functions will generate thick disks with well-defined properties; see [31] for a detailed discussion. Also, we should have

$$a \ge \frac{2nb}{2n + 1 - bc}, \qquad \text{and} \quad 0 \le bc < 2n + 1. \qquad (31)$$

Note that, unlike the transformation presented in Sec. III A, the functions defined by Eq. (30) will generate disks with finite thickness located between $-b \le z \le b$.

As an example we show in Figs. 4(a)–4(d) level curves of the energy density $\bar{\epsilon}$ and the effective Newtonian density $\bar{\rho}$ with parameters $n = 1$, $\bar{a} = 2$, $\bar{c} = 0$, $\bar{m} = 1$, $\bar{\alpha} = 0.1$ in Fig. 4(a) and 4(c) and $\bar{\alpha} = 0.9$ in Fig. 4(b) and 4(d) where now all quantities are rescaled in terms of b. Again there is no heat flow, and the density distributions are everywhere non-negative and free from singularities. Figures 5(a)–5(d) display some level curves of the azimuthal stress and vertical pressure, respectively, with the same parameters. The qualitative features of the azimuthal stress and the influence of the Kerr parameter on the disk's properties are very similar to the rotating disk presented in Sec. III A. The dominant energy condition is also satisfied: for $\tilde{\alpha} = 0.1$ we have $|\tilde{P}_\varphi/\tilde{\epsilon}| < 0.4$, $|\tilde{P}_z/\tilde{\epsilon}| < 0.1$; for $\tilde{\alpha} = 0.9$ we have $|\tilde{P}_\varphi/\tilde{\epsilon}| < 0.3$ and $|\tilde{P}_z/\tilde{\epsilon}| < 0.06$. Some curves of

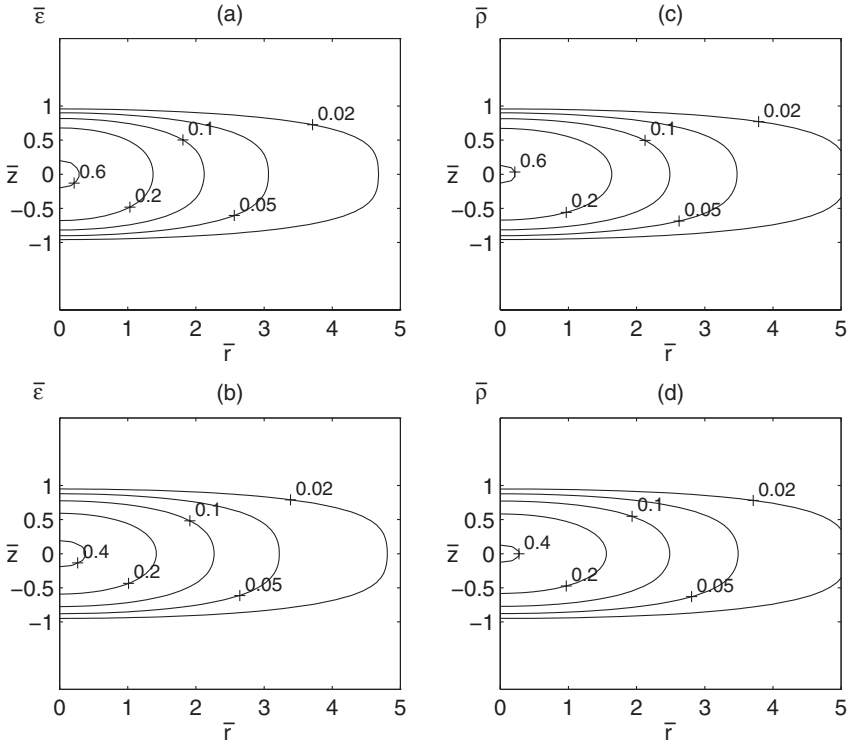

FIG. 4. For the second family of thick Kerr disks, we show level curves of the energy density $\bar{\epsilon}$ as functions of $\bar{r}$ and $\bar{z}$ with parameters $n = 1$, $\bar{a} = 2$, $\bar{c} = 0$, $\bar{m} = 1$, $\bar{\alpha} = 0.1$ in (a) and $\bar{\alpha} = 0.9$ in (b). The effective Newtonian density $\bar{\rho}$ with the same parameters is shown in (c) and (d).

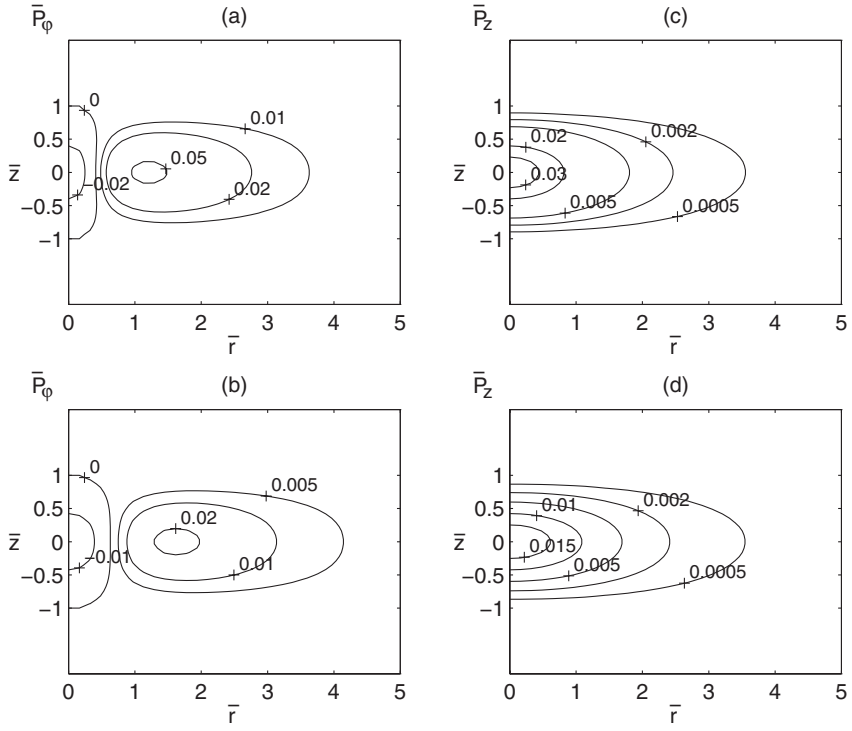

FIG. 5. For the second family of thick Kerr disks, we show level curves of the azimuthal stress $\bar{P}_{\varphi}$ as functions of $\bar{r}$ and $\bar{z}$ with parameters $n = 1$, $\bar{a} = 2$, $\bar{c} = 0$, $\bar{m} = 1$, $\bar{\alpha} = 0.1$ in (a) and $\bar{\alpha} = 0.9$ in (b). The vertical pressure $\bar{P}_z$ with the same parameters is shown in (c) and (d).

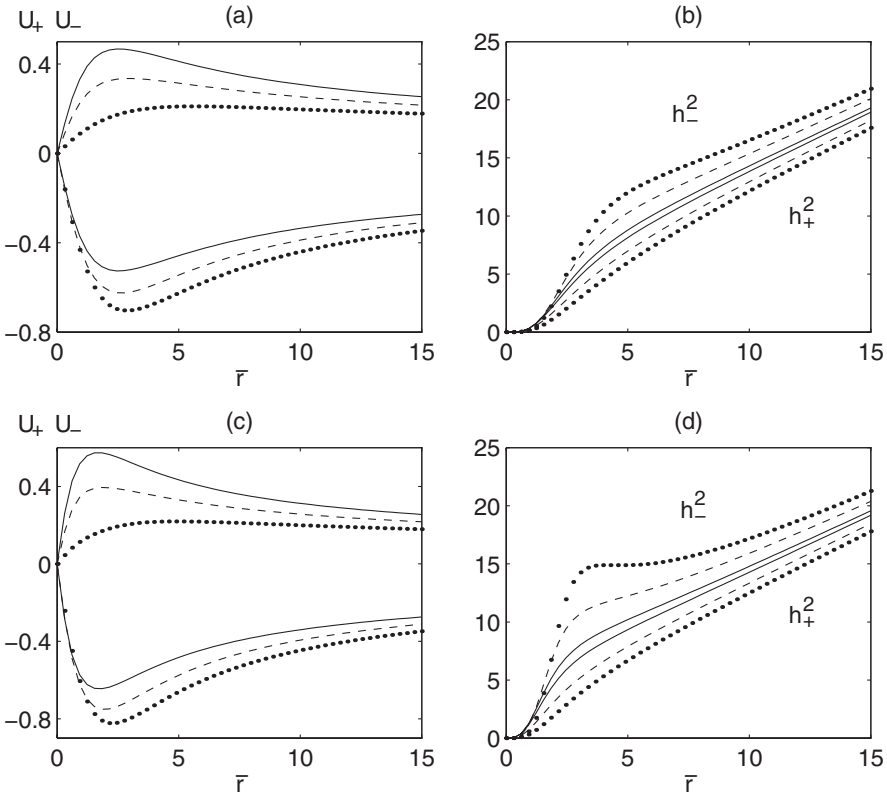

FIG. 6. For the second family of thick Kerr disks, we show curves of the prograde U_+ and retrograde U_- tangential velocities and the square of angular momenta h_-^2 and h_+^2. Parameters: $n = 1$, $\bar{c} = 0$, $\bar{m} = 1$, $\bar{\alpha} = 0.1$ (solid lines), $\bar{\alpha} = 0.5$ (dashed lines), $\bar{\alpha} = 0.9$ (dotted lines), $\bar{a} = 2$ in (a) and (b) and $\bar{a} = 1.5$ in (c) and (d).

prograde and retrograde tangential velocities are shown in Fig. 6(a) and of the square of angular momenta in Fig. 6(b) with parameters $n = 1$, $\bar{c} = 0$, $\bar{a} = 2$, $\bar{m} = 1$, $\bar{\alpha} = 0.1$ (solid lines), $\bar{\alpha} = 0.5$ (dashed lines), and $\bar{\alpha} = 0.9$ (dotted lines); and in Figs. 6(c) and 6(d) $\bar{a} = 1.5$. In 6(d) we note again a small instability region for the retrogade orbit with $\bar{\alpha} = 0.9$.

IV. DISCUSSION

We presented two families of exact general relativistic rotating thick disks which were obtained by applying different transformations on the Kerr metric. The first was a Miyamoto-Nagai–like one, and the second was based on the "displace, cut, fill and reflect" method. Both transformations generate disks with similar properties. The energy density and "effective" Newtonian density are free from singularities and also are non-negative for several values of the parameters tested, thus satisfying the strong as well as the weak energy conditions. They present azimuthal tensions near the center and pressures for larger values of the radial and vertical coordinates, and the vertical pressures have the same modulus as the radial tensions. For the examples studied, the dominant energy condition was also satisfied. In general, the effect of rotation is to decrease the maximum values of the density distributions near the origin and make them slightly flattened. Rotation also reinforces the asymmetry of the prograde and retrogade rotation curves on the $z = 0$ plane, and large values of the Kerr parameter destabilize high relativistic orbits (mostly retrogade).

Although our examples of rotating disks based on the Kerr metric do not have heat flow, an analytical proof that the discriminant equation (13) is never negative is not trivial. A more complete study of stability of these disk models by using conservation equations from perturbations of the energy-momentum tensor would also be a challenging task.

ACKNOWLEDGMENTS

D. V. thanks FAPESP for financial support. P. S. L. thanks CNPq and FAPESP for financial support.

[1] W. A. Bonnor and A. Sackfield, Commun. Math. Phys. **8**, 338 (1968).
[2] T. Morgan and L. Morgan, Phys. Rev. **183**, 1097 (1969).
[3] L. Morgan and T. Morgan, Phys. Rev. D **2**, 2756 (1970).
[4] G. González and P. S. Letelier, Classical Quantum Gravity **16**, 479 (1999).
[5] D. Lynden-Bell and S. Pineault, Mon. Not. R. Astron. Soc. **185**, 679 (1978).
[6] P. S. Letelier and S. R. Oliveira, J. Math. Phys. (N.Y.) **28**, 165 (1987).
[7] J. P. S. Lemos, Classical Quantum Gravity **6**, 1219 (1989).
[8] J. P. S. Lemos and P. S. Letelier, Classical Quantum Gravity **10**, L75 (1993).
[9] J. Bičák, D. Lynden-Bell, and J. Katz, Phys. Rev. D **47**, 4334 (1993).
[10] J. Bičák, D. Lynden-Bell, and C. Pichon, Mon. Not. R. Astron. Soc. **265**, 126 (1993).
[11] J. P. S. Lemos and P. S. Letelier, Phys. Rev. D **49**, 5135 (1994).
[12] J. P. S. Lemos and P. S. Letelier, Int. J. Mod. Phys. D **5**, 53 (1996).
[13] G. González and O. A. Espitia, Phys. Rev. D **68**, 104028 (2003).
[14] G. García and G. González, Phys. Rev. D **69**, 124002 (2004).
[15] J. Bičák and T. Ledvinka, Phys. Rev. Lett. **71**, 1669 (1993).
[16] G. González and P. S. Letelier, Phys. Rev. D **62**, 064025 (2000).
[17] P. S. Letelier, Phys. Rev. D **60**, 104042 (1999).
[18] J. Katz, J. Bičák, and D. Lynden-Bell, Classical Quantum Gravity **16**, 4023 (1999).
[19] D. Vogt and P. S. Letelier, Phys. Rev. D **68**, 084010 (2003).
[20] D. Vogt and P. S. Letelier, Phys. Rev. D **70**, 064003 (2004).
[21] V. Karas, J. M. Huré, and O. Semerák, Classical Quantum Gravity **21**, R1 (2004).
[22] C. Klein, Classical Quantum Gravity **14**, 2267 (1997).
[23] G. Neugebauer and R. Meinel, Phys. Rev. Lett. **75**, 3046 (1995).
[24] C. Klein and O. Richter, Phys. Rev. Lett. **83**, 2884 (1999).
[25] C. Klein, Phys. Rev. D **63**, 064033 (2001).
[26] J. Frauendiener and C. Klein, Phys. Rev. D **63**, 084025 (2001).
[27] C. Klein, Phys. Rev. D **65**, 084029 (2002).
[28] C. Klein, Phys. Rev. D **68**, 027501 (2003).
[29] C. Klein, Ann. Phys. (N.Y.) **12**, 599 (2003).
[30] G. González and P. S. Letelier, Phys. Rev. D **69**, 044013 (2004).
[31] D. Vogt and P. S. Letelier, Phys. Rev. D **71**, 084030 (2005).
[32] M. Miyamoto and R. Nagai, Publ. Astron. Soc. Jpn. **27**, 533 (1975).
[33] R. Nagai and M. Miyamoto, Publ. Astron. Soc. Jpn. **28**, 1 (1976).
[34] D. Vogt and P. S. Letelier, Mon. Not. R. Astron. Soc. **363**, 268 (2005).
[35] Lord Rayleigh, Proc. R. Soc. A **93**, 148 (1917); see also L. D. Landau and E. M. Lifshitz, *Fluid Mechanics* (Pergamon Press, Oxford, 1987), 2nd ed., Sec. 27.
[36] P. S. Letelier, Phys. Rev. D **68**, 104002 (2003).
[37] M. Ujevic and P. S. Letelier, Phys. Rev. D **70**, 084015 (2004).
[38] M. Ujevic and P. S. Letelier, Gen. Relativ. Gravit. **39**, 1345 (2007).
[39] S. W. Hawking and G. F. R. Ellis, *The Large Scale Structure of Space-Time* (Cambridge University Press, Cambridge, England, 1973).